Supplementary information for

Projected future changes of tropical cyclone genesis frequency in the Northern Hemisphere based on a multi-timescale regression model

Jiuwei Zhao[1,2,3], Ruifen Zhan[1,4,5*], Yuqing Wang[3*], Leishan Jiang[3] and Xin Huang[4]

[1]Department of Atmospheric and Oceanic Sciences & Institute of Atmospheric Sciences, Fudan University, Shanghai, China

[2]School of Atmospheric Science, Nanjing University of Information Science & Technology (NUIST), Nanjing, China

[3]International Pacific Research Center and Department of Atmospheric Sciences, School of Ocean and Earth Science and Technology, University of Hawaii at Mānoa, Honolulu, Hawaii, USA.

[4]Shanghai Typhoon Institute, China Meteorological Administration, Shanghai, China

[5]CMA-FDU Joint Laboratory of Marine Meteorology, Shanghai, China

*Corresponding authors: Dr. Ruifen Zhan (Email: zhanrf@fudan.edu.cn), Dr. Yuqing Wang (Email: yuqing@hawaii.edu)

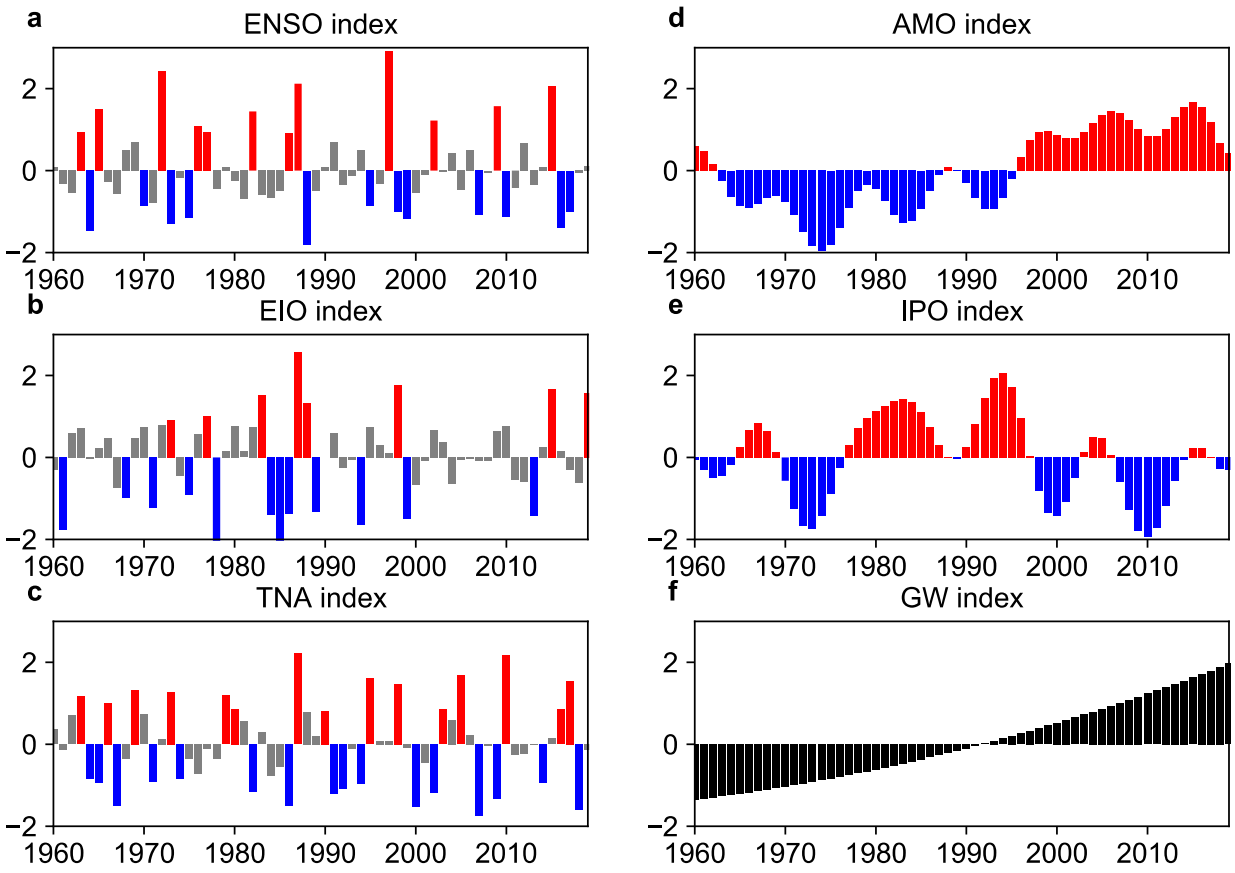

Supplementary Figure 1. Normalized time series of the Nino3.4, EIO, TNA, IPO, AMO and GW indices from 1960–2020. The red (blue) bars in the left panel represent the positive and negative events reaching 0.8 standard deviation. The red and blue colors in (d) and (e) represent the corresponding positive and negative IPO and AMO phases. The normalized CO_2 warming trend is shown in (*F*).

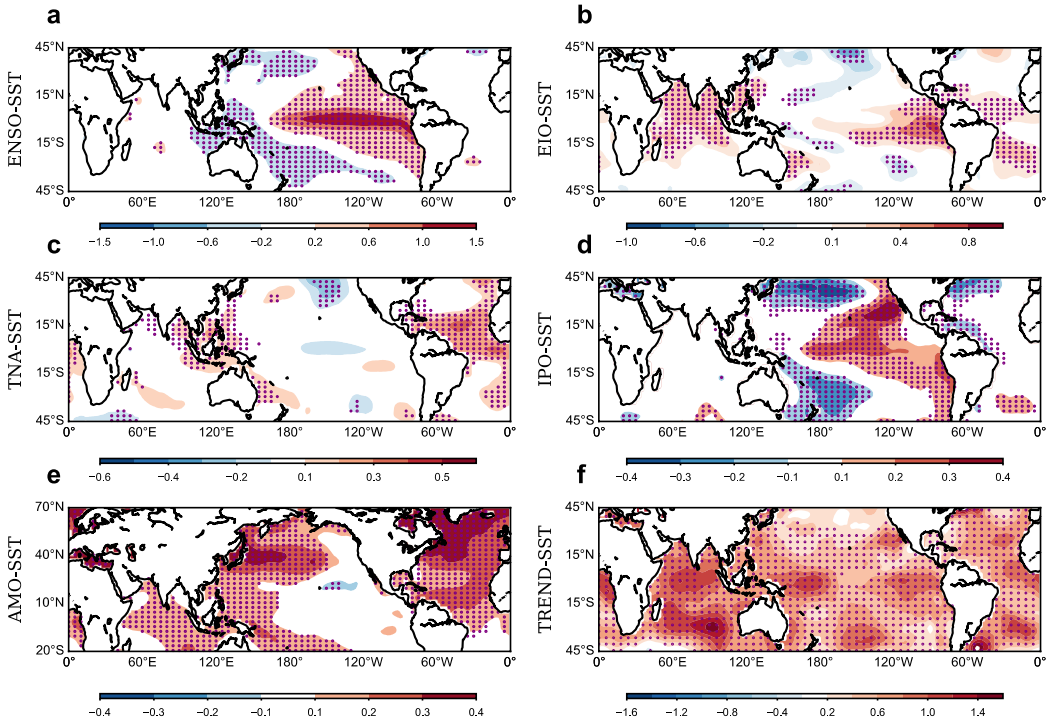

Supplementary Figure 2. The composite differences and linear trend increments of SST (ºC). Differences in SST between (a) El Niño and La Niña events, (b) positive and negative EIO events, (c) positive and negative TNA events, (d) positive and negative IPO phases, (e) positive and negative AMO phases; and (f) linear trend increments of SST from 1960–2019. The dots in (a-e) represent the areas where the statistical significance is above 90% confidence level based on the student's t test while the dots in (f) stand for the areas where the statistical significance is above 90% confidence level based on the Mann-Kendall trend test.

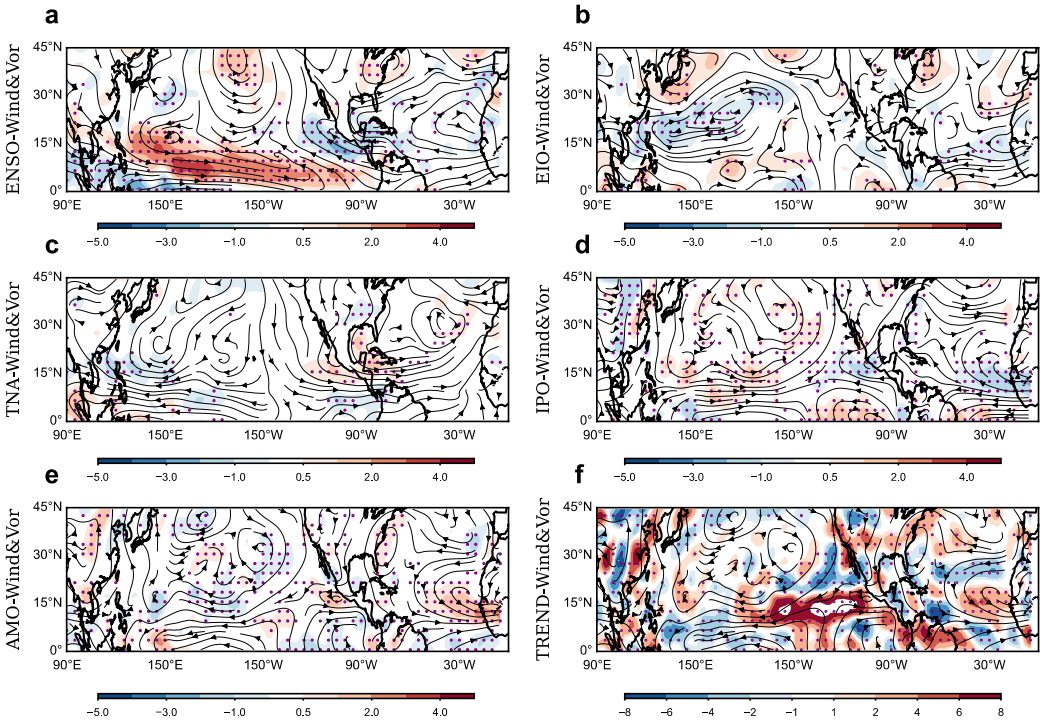

Supplementary Figure 3. The composite differences and linear trend increments of 850 hPa winds (m s^{-1}) and vorticity anomalies (10^{-5} s^{-1}). Differences between (a) El Niño and La Niña events, (b) positive and negative EIO events, (c) positive and negative TNA events, (d) positive and negative IPO phase, (e) positive and negative AMO phase; and (f) linear trend increments from 1960–2019. The dots in (a-e) represent the areas of vorticity above 90% confidence level based on the student's t test while the dots in (f) stand for the areas of vorticity above 90% confidence level based on the Mann-Kendall trend test.

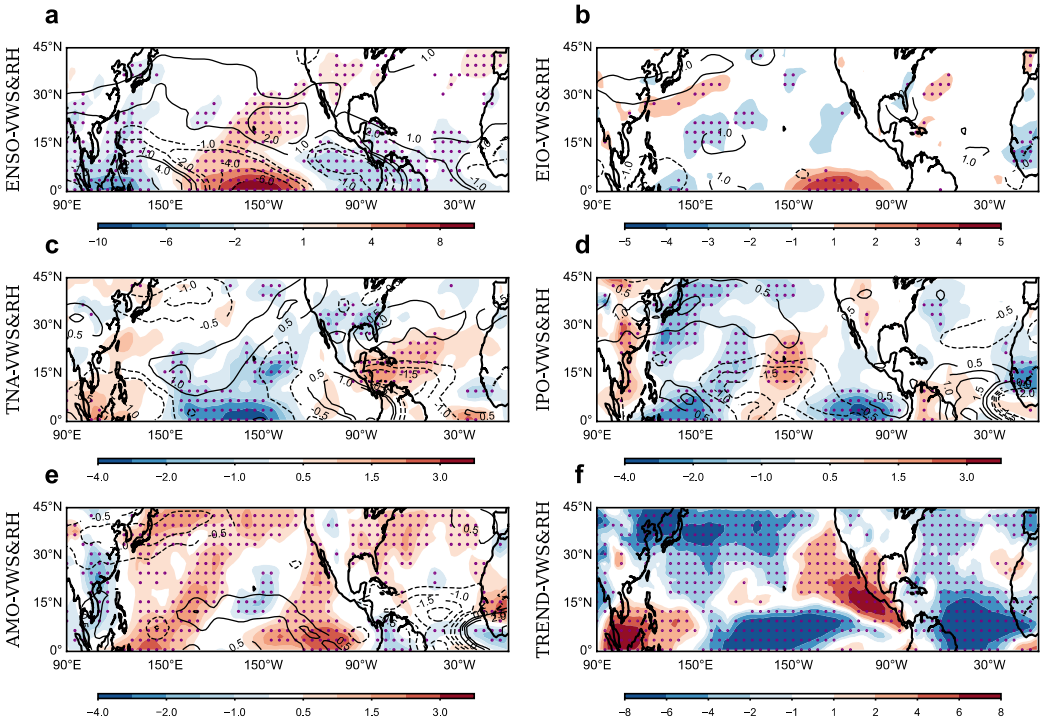

Supplementary Figure 4. Same as Supplementary Figure 3 but for RH (%, shaded) and VWS (m s^{-1}, contours).

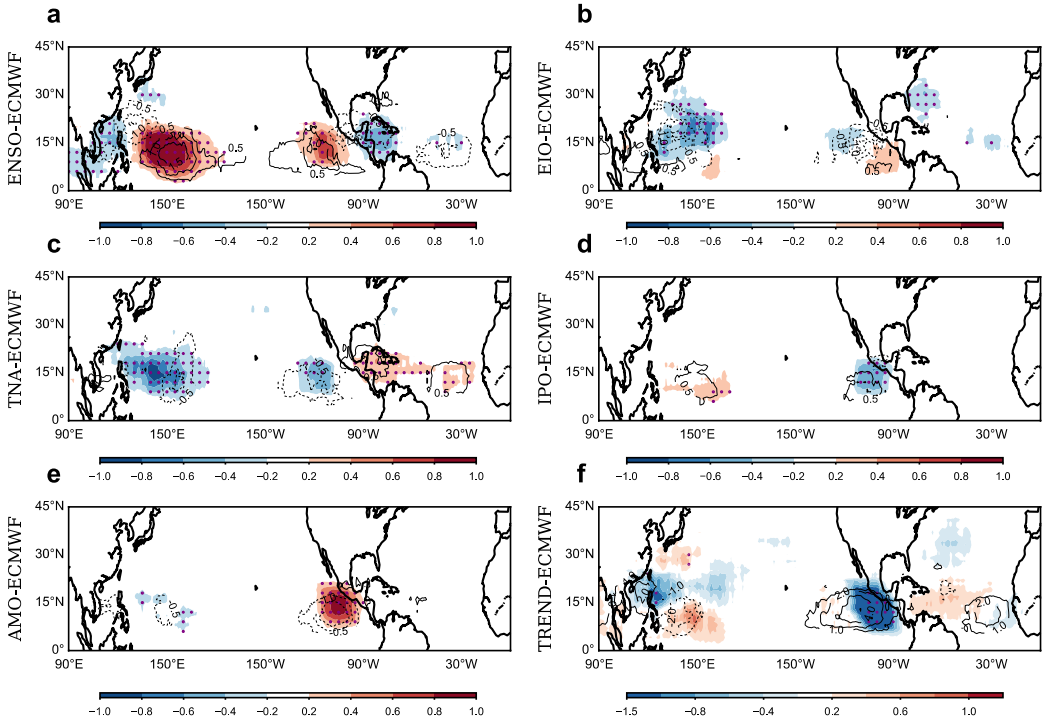

Supplementary Figure 5. **The connections of the observed and multi-model ensemble TCGF from the ECMWF-IFS (5 members) for the period 1960-2014.** Composite differences of the observed (shaded) and simulated (contours) TCGF between (a) El Niño and La Niña years, (b) positive and negative EIO events, (c) positive and negative TNA events, (d) positive and negative IPO phases, (e) positive and negative AMO phases; (f) linear trend increments from 1960–2014. The dots in (a-e) represent the areas statistically significant above 90% confidence level based on the student's t test, and those in (f) stand for the areas statistically significant above 90% confidence level based on the Mann-Kendall trend test.

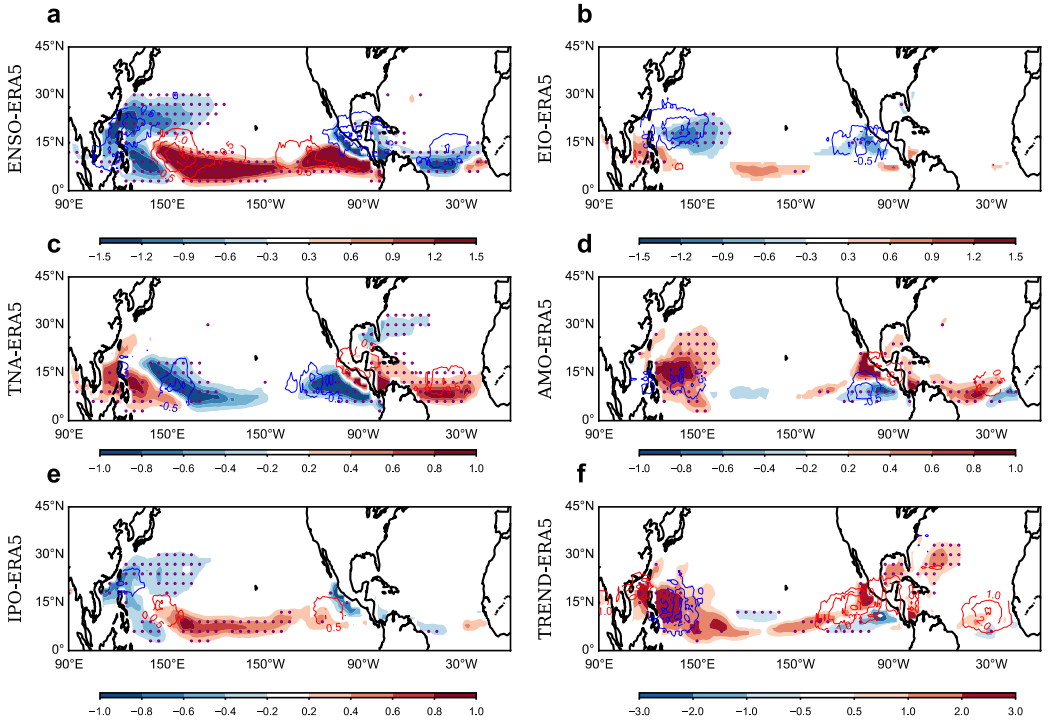

Supplementary Figure 6. **The connections of the observed TCGF and commonly used GPI based on the ERA5 dataset with the six key factors used in regression model for the period 1960-2018.** The composite differences between (*a*) El Niño and La Niña events, (*b*) positive and negative EIO events, (*c*) positive and negative TNA events, (*d*) positive and negative IPO phases, (*e*) positive and negative AMO phases; and (*f*) the linear trend increments from 1960 to 2018. The dots indicate the areas where the differences are statistically significant at the 95% confidence level by the Student's t test. The contours represent the observed TCGF and the shades stand for the GPI.

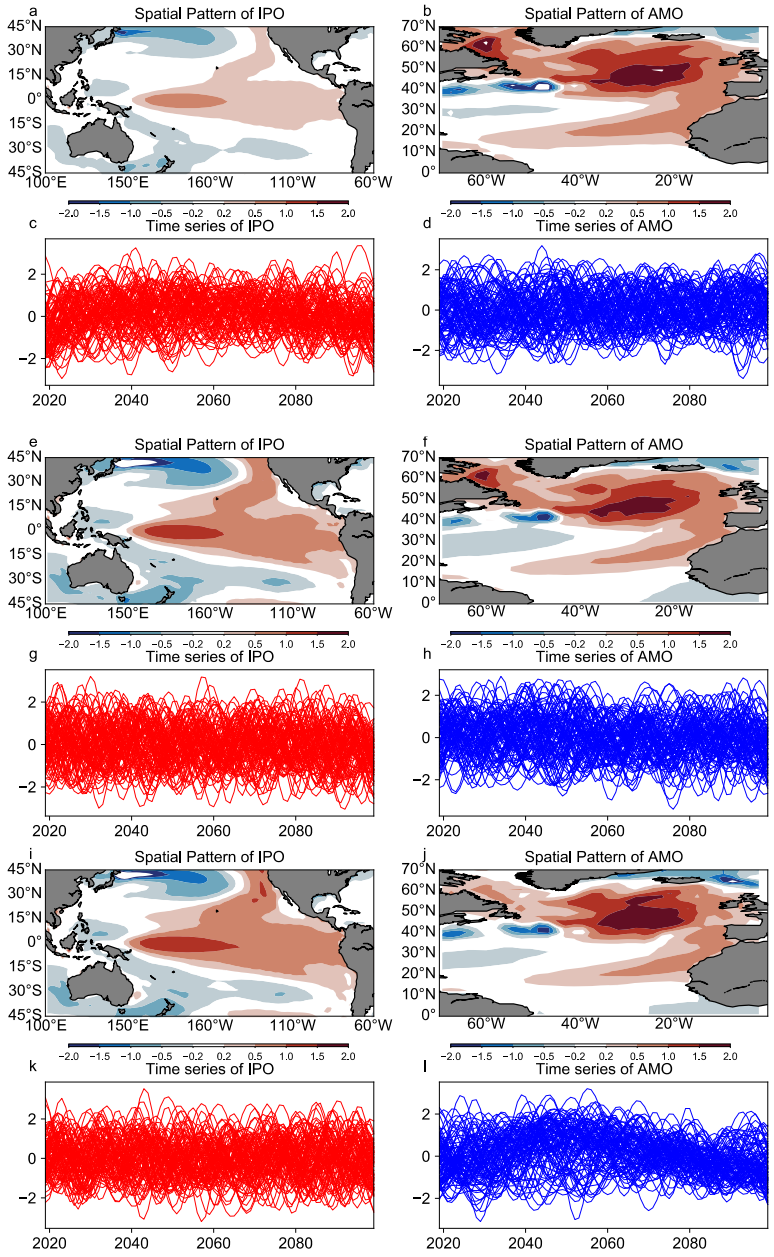

86

87 **Supplementary Figure 7. The spatial patterns of the IPO and AMO and their corresponding**
88 **principal components derived from 100 ensemble members of the MPI-ESM SST data**
89 **for RCP2.6 (a-d), RCP4.5 (e-h) and RCP8.5 (i-l) scenarios, respectively.** (a) The spatial
90 patterns of (a) IPO and (c) AMO both obtained from the second EOF mode in respective basins;
91 (b) normalized time series of the IPO from 100 members; and (d) normalized time series of
92 the AMO from the second principal component for RCP2.6 scenario; (e-h), same as (a-d) but
93 for RCP4.5 scenario; (i-l) same as (a-d) but for RCP8.5 scenario. Here, the spatial pattern is
94 averaged based on 100 members that were converted to the positive phase.

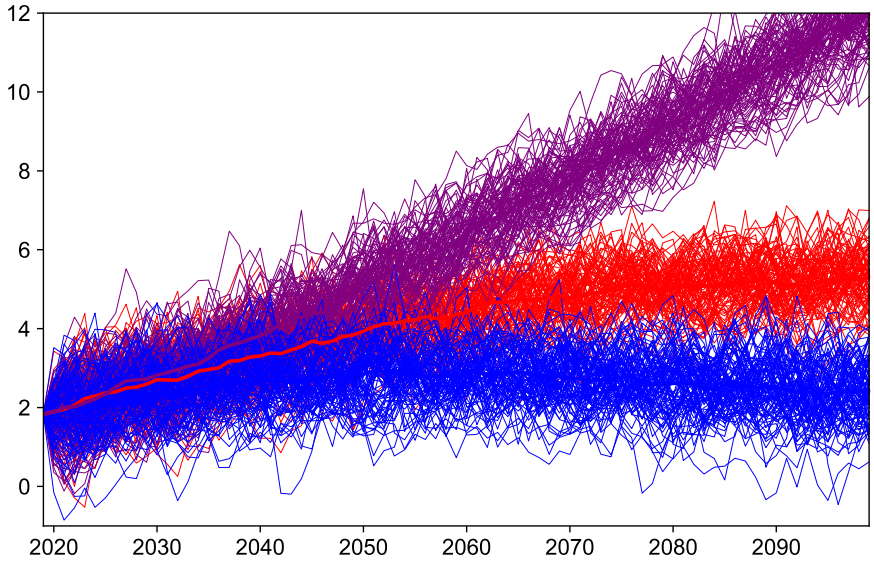

Supplementary Figure 8. The time series of GMSST from 2019-2099. Here, the time series from 1949-2019 is derived from NOAA SST averaged over 45ºS-45ºN, 0º-360º. The time series from 2019-2099 are derived from 100 ensemble of MPI-ESM models. The purple, red and blue lines represent 100 members in RCP8.5, RCP4.5 and RCP2.6 scenarios, respectively. The thick lines indicate the ensemble mean in each of the scenarios.